MDPI

Article

Analysis of Diabetic Retinopathy (DR) Based on the Deep Learning

Abdul Muiz Fayyaz [1], Muhammad Imran Sharif [2], Sami Azam [3,*], Asif Karim [3] and Jamal El-Den [3]

[1] Department of Computer Science, University of Wah, Wah 47040, Pakistan
[2] Department of Computer Science, COMSATS University Islamabad, Wah 47040, Pakistan
[3] Faculty of Science and Technology, Charles Darwin University, Darwin 0909, Australia
* Correspondence: sami.azam@cdu.edu.au

Abstract: If Diabetic Retinopathy (DR) patients do not receive quick diagnosis and treatment, they may lose vision. DR, an eye disorder caused by high blood glucose, is becoming more prevalent worldwide. Once early warning signs are detected, the severity of the disease must be validated before choosing the best treatment. In this research, a deep learning network is used to automatically detect and classify DR fundus images depending on severity using AlexNet and Resnet101-based feature extraction. Interconnected layers helps to identify the critical features or characteristics; in addition, Ant Colony systems also help choose the characteristics. Passing these chosen attributes through SVM with multiple kernels yielded the final classification model with promising accuracy. The experiment based on 750 features proves that the proposed approach has achieved an accuracy of 93%.

Keywords: deep learning; classification; diabetic retinopathy; AlexNet; Resnet101

1. Introduction

The advances in science and technology have improved the standard of living for humans by making their lives easier, safer, and more convenient to live [1]. Machine Learning (ML) [2,3]-based automated systems these days provide a variety of services to customers, all with the goal of improving the quality of our lives. ML-based systems have become quite significant in the accurate early detection of dangerous diseases. One of the most common and debilitating conditions affecting people all over the globe is diabetic retinopathy (DR) [4,5]. It is a major contribution to the increase in the frequency of vision disorders among individuals, which is the major driving force behind the general rise in the number of people who are experiencing vision loss. People who are diagnosed with DR have an approximately 90% chance of averting the permanent loss of their vision if early diagnosis is performed correctly and effectively [6].

The clinical, blood-vascular, and optic disc features of a patient may be improved using image enhancement technologies for retinal imaging [7]. A typical visual diagnostic approach for DR diagnosis is digital fundus imaging. Recent clinical studies recommend carrying out this check on a consistent basis throughout the whole of the diabetic patient's life. Patients who had none or a mild degree of diabetic retinopathy, for instance, were instructed to go through screening once a year, but those who had moderate retinopathy were instructed to repeat fundus examinations every six months. This retinal examination, along with the overall rise in the number of DR patients throughout the globe, represents a huge responsibility that medical professionals consider difficult to handle [8,9]. Due to various recent developments in areas such as nonmydriatic eye imaging and online data transmission, it is now feasible to use retinal fundus image analysis (RFIA) systems for the purpose of analyzing the retinal image in order to make a diagnosis of DR. The phases of the retinography sample analysis procedures may be carried out by qualified eye physicians or non-eye trained personnel, depending on the results corresponding to

acquired sensitivity (SE) and specificity (SP). The usual performance of automated software for the diagnosis of diabetic retinopathy is outstanding, with sensitivity (SE) approaching 80% and specificity (SP) reaching 95% [10,11].

Screening programmers will need to take more retinal image graphs as the number of diabetes patients continues to rapidly increase [12]. This will create a high demand for medical personnel and will drive up the cost of healthcare services. It is possible that a computerized system may be of use here, either as a resource for making comprehensive technological diagnoses or as a back-up for the efforts of medical doctors [13,14]. An automated system must be able to classify retinal images in a professional manner using severity ratings that are currently being used in clinical settings. The proposed international clinical diabetic retinopathy and diabetic macular edema disease scales are two examples of these severity ratings [15–17]. There are two distinct flavors of DR, Non-Proliferative Diabetic Retinopathy (NPDR), the less severe form, and Proliferative Diabetic Retinopathy(PDR), the more severe form [18]. The signs of a DR are the first symptoms that manifest themselves. These symptoms could include a mild illness or NPDR. Patients who have NPDR may initially have just foggy vision in the early stages of the disease; but, as the disorder advances, the retina starts to generate new blood vessels, which may result in significant visual impairment [19]. Diabetes mellitus is a condition that is caused by excessive levels of blood sugar, which results in the vessels expanding and leaking fluid [20]. In the images of the fundus retina, the lesions seem like dots of streaming blood and fluids. There are two distinct sorts of lesions, which are referred to, respectively, as bright lesions and red lesions [21]. Red lesions include microaneurysms (MCA) and hemorrhage (HM), while bright lesions contain soft and hard exudates. Both types of exudates may be seen in bright lesions (EX). HM and MCA are represented, respectively, by the bigger and smaller dark red dots. Hard EX is displayed as vivid yellow spots, but soft EX, often known as cotton wool, manifests as fluffy, yellowish-white patches. This is because soft EX causes damage to nerve fibers, whereas hard EX does not [22,23]. Research has shown that an automated system that is based on the technology of deep learning ay be able to diagnose diabetic retinopathy successfully [24].

The Major Contributions Are as Follow

- In preprocessing, the resize function is used to scale all the images to 1000×1000 pixels since the images' dimensions vary. After resizing, k-mean clustering is used to enhance the image. We used a variety of data augmentation techniques to boost the quantity of low-volume data while dealing with the original dataset. These strategies included vertical and horizontal flips as well as 90-degree and 180-degree rotations.
- To achieve features, AlexNet and Resnet101 are utilized. The characteristics are extracted from the fully connected layers.
- Serial feature fusion is used to fuse these extracted features.
- Several of these features are insignificant for successful classification; hence, we used an efficient feature selection method known as Ant Colony system to choose the most beneficial features to include in our classification. Afterwards, these selected attributes are sent to SVM with several kernels for final classification.

The article is organized as follows: Section 2 provides an explanation of relevant work, including more modern methodologies. In Section 3, we describe the technique that has been presented. The outcomes of the suggested research approach are discussed in Section 4.

2. Related Work

The researchers [25] used a two-stage method for automated DR classification. First, two U-Net models are utilized to segment the OD and blood vessels (BV). Second, a symmetric hybrid CNN-SVD model was created to detect DR by recognizing microaneurysms, hemorrhages, and exudates. After OD and BV extraction, this model was preprocessed to pick the most discriminant features using Inception-V3 and transfer learning (EX). In [26],

authors presented an advanced framework for the classification of diabetic retinopathy that focuses on feature selection over deep features and used wrapper approaches that were inspired by nature. In [27], for the fundus image evaluation, targeted contrastive learning was applied to determine the severity of diabetic retinopathy. DR is the most challenging eye ailment diabetes sufferers may encounter. A considerable proportion of people may escape the permanent stage of the illness, which is blindness, if DR is detected early. The artificial intelligence-based systems that have been developed are accurate in their identification of DR and exhibit promising outcomes. Numerous discoveries have been made in this sector, which is now a very active and popular area of research.

A technique that is based on classical ML and DL [27] is proposed for use in the categorization of patient retinal fundus images into classes according to the severity level of the illness. They used a CNN architecture that had been trained using Transfer Learning and was driven by deep learning in order to finalize the classification. In order to do multi-label categorization [28] of fundus illness, binocular fundus images were used with a neural network algorithm model. This was conducted with the intention of improving accuracy. The model was constructed using attention processes and the fusing of different features. Binocular fundus images are focused on certain features by the algorithm, which then feeds them into a ResNet50 network that has attention mechanisms built in. This allows the attributes of the fundus image lesions to be extracted. In this study [29], image classification and identification of the retinal fundus were suggested employing cutting-edge deep learning approaches in supervised, self-supervised, and vision transformer setups. They investigated, assessed, and summed up the three different types of diabetic retinopathy, which are referable, non-referable, and proliferative. The strategy that has been presented aims to solve the issue of poor fundus image quality and identify the indicators of retinopathy. WFDLN processes two channels of fundus images, which are referred to as contrast-limited adaptive histogram equalization (CLAHE) fundus images and contrast-enhanced canny edge detection (CECED) fundus images. In the case of the CECED fundus images, the features are recovered using fine-tuned Inception V3, but in the case of the CLAHE fundus images, fine-tuned VGG-16 is used to extract the features of the image. A weighted technique is used to aggregate the outputs from both channels, and the final recognition result is obtained using a SoftMax classification. The examination of the experimental findings revealed that the network could reliably recognize the DR phases [30].

The primary focus of this was on the difficulty of segmenting the fundus images of newborn babies who had been delivered preterm. They used two different approaches to create the novel dataset of the participants; these approaches were dissimilar from one another in terms of their size, resolution, and illumination, respectively.

The trained models demonstrated a high degree of adaptation and resilience in the face of heterogeneity and unpredictability in the data because of this. They were able to achieve superior U-Net topologies by combining squeeze and excitation (SE) blocks with attention gates (AG) to isolate the demarcation line/ridge and vessel from the datasets. This resulted in the desired separation. Because of this, they were able to divide the demarcation line/ridge and the vessel. Employing a deep learning (DL) learning-based automated system and executing retinal fundus image classification methods led to the discovery of diabetic retinopathy. They devised efficient answers to the issues, complications, and challenges that surfaced in the modern era of autonomous systems [31–33].

The combination of fundus images and image processing that is based on deep learning allowed for the diagnosis of diabetic retinopathy and other retinal issues [34]. In addition, diagnosing DR manually is difficult since it may disturb the retina, leading to structural changes such as microaneurysms (MAs), exudates (EXs), and hemorrhages (HMs), as well as the creation of extra blood vessels. The detection and classification of diabetic retinopathy in fundus images of the eye is accomplished via the use of a hybrid technique that is proposed here. Transfer learning is performed on CNN models that have already been trained, and it is used to extract features, which are then blended to generate a hybrid

feature vector. This feature vector is used by a number of classifiers for the purpose of performing binary and multiclass classification on fundus images [35].

3. Proposed Methodology

In our research, a unique and effective deep learning-based framework for the categorization of diabetic retinopathy is presented. The fundus image dataset [35] is used for analysis of diabetic retinopathy. Accordingly, the images are exported in a variety of dimensions and in a low quantity, and the resize function is used during the preprocessing step to scale each of the images to a resolution of 1000 pixels on each end. Using the initial dataset, we carried out several different data augmentation processes in order to increase the amount of low-volume data that was made accessible for analysis. These concepts include, among others, inverting the vertical and horizontal axes, rotating 90 degrees, and rotating 180 degrees. The AlexNet and Resnet101 are utilized for feature extraction. The characteristics are extracted from the fully connected layers that are completely related to one another. Ant Colony algorithm is used for selecting core features. The final classification is determined by running these chosen characteristics through several kernels of a support vector machine (SVM). The proposition's general design is shown in Figure 1.
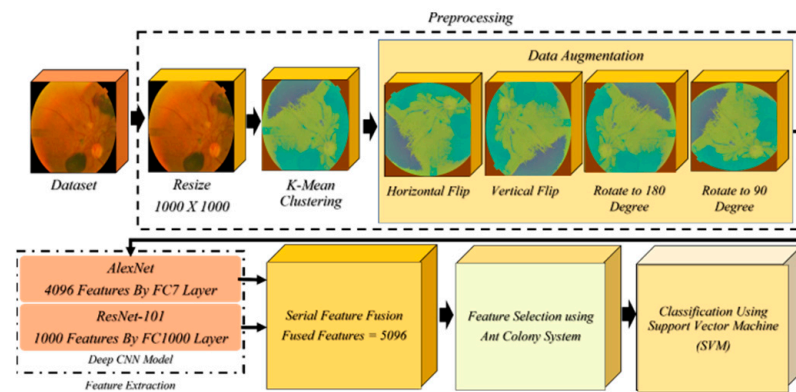

Figure 1. Describes the architecture of proposed methodology.

3.1. Resizing and Data Augmentation

To begin, we perform preprocessing operations on the input images, including resizing [36] and k-mean clustering. After being shrunk down, each section of the matrix appears as a discrete dot on the screen. In a true color image, the intensity of the red pixels is represented on the first bigger plane, the intensity of the green pixels is shown on the second level, and the intensity of the blue pixels is displayed on the third level. This strategy allows us to show off two actions in the column without sacrificing any image quality, no matter how narrow the column is. Note that just the first two dimensions of the provided image need to change. K-mean clustering [37] is used for enhancing the image as shown in Figure 2. Because the datapoints in k-means are far fewer than the total clusters, each datapoint is referred to as the cluster's centroid on the graph. Each centroid is associated with a cluster number. If there are more datapoints than clusters, the distance between each datapoint and each centroid is calculated, resulting in the shortest feasible distance. This data sample is stated to be a member of the cluster that is the shortest distance away from this data. Its mathematically express as [37].

$I = (I_1, I_2)$ and $J = (J_1, J_2)$ are the points, then the distance is given by:

$$Distance(I\&J) = \sqrt{(I_1 - J_1)^2 + (I_2 - J_2)^2} \tag{1}$$

The cluster centroid is symbolized by k_i, x is the datapoint that is assigned to each cluster. Here Dist is the euclidean distance as shown in Equation (2):
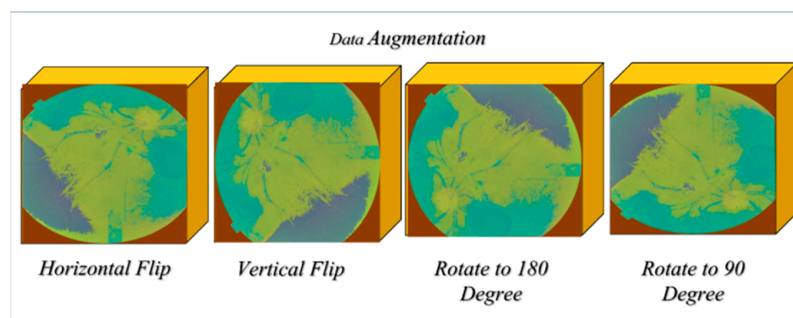
$$minimum\_Dist(k_i, x) \tag{2}$$

Figure 2. Illustrates the data augmentation.

Multiple data augmentation methods were used on the original dataset in order to increase the sparse data, such as flipping the dataset vertically, horizontally, 90 degrees, or 180 degrees [38,39]. The results of the research were used to assess and categorize DR in medical imaging. This dataset is also known as a "vertically flipped dataset" since it is comprised of images from the original dataset that have been rotated vertically to change the location of a diabetic retinopathy patch within the image's graphs. Both the "action" and "axis" parameters were set to the value "flip", and the "axis" parameter was set to "vertical". Both the "action" and "axis" parameters have been optimized to their maximum potential. Since the new flip vertical dataset was much larger than the original images dataset, the two were combined to produce a dataset twice as large. As described above, the horizontally flipped dataset was produced by rotating each image in the original dataset by 90 degrees, shifting the location of the diabetic retinopathy patch in each image. Action was set to "flip" and axis was set to "horizontal" in the transformation such that the image was flipped vertically. The dataset size needed to be increased; thus, the produced flipped-horizontal dataset was joined with the original images' dataset. The images from the original dataset were rotated 90 degrees counterclockwise to produce the 90-degree rotation dataset. The output images needed to be shown on the screen at an exact angle of 900 degrees; thus, the value of the parameter "action" was set to "rotate", and the min/max degrees tags in the settings tags were set to 900 degrees. To expand the size of the original dataset, the produced dataset was combined with a dataset comprising the original images.

The images in the original dataset were rotated by 180 degrees and then combined to form the 180-degree rotation dataset. Since the generated images were rotated to be precisely at an angle of 1800 degrees, the value of the "action" parameter was set to "rotate", and the min/max degrees tags in the settings tags were set to 1800 and 1800 degrees, respectively. To expand the size of the original dataset, the produced dataset was combined with a dataset comprising the original images. Figure 2 describes the data augmentation.

3.2. Feature Extraction

Convolutional neural networks, such as AlexNet and Resnet101 [40–42], are used to recognize images. With the ImageNet database, we can load a version of the network that has already been trained on more than a million images. The pretrained network can put images into more than 1000 categories. It can also put images into a wide range of animal categories, as well as categories for keyboards, mice, and pencils. Because it has been trained in this way, the network has learned to represent a wide range of image types using many different features. The Resnet101 network will accept images with a resolution of 224 by 224 pixels. The AlexNet network will accept images with a resolution of 227 by 227 pixels. To be more specific, we took the diabetic retinopathy dataset and used AlexNet and RESNET101 to pull out the most important features. We used the FC7 fully connected layer of the AlexNet, which had 4096 features, and the FC1000 fully connected layer of the Resnet101, which had 1000 features.

3.2.1. AlexNet Deep CNN Model

Krizhevsky and his team proposed 8-layer deep architecture called AlexNet [43]. The AlexNet contain five deep convolution layers and three fully connected layers. This network uses the rectified linear unit (ReLU) function instead of the sigmoid function to deal with the problem of vanishing gradients and to train quickly. The pooling operation is used to cut down on the size of the space. The size of the fully connected layers (FC6 and FC7) is 4096 features. For the last fully connected layer, which is called the "output layer", the size of the FC8 is 1000 features.

3.2.2. ResNet-101 Deep CNN Model

ResNet-101 [44] is a 152-layer deep neural network. ResNet-101 developed the concept of integrating residual mapping with network layers. It stacks residual blocks, with each residual block consisting of two 3×3 convolutional layers. ResNet-101 altered CNN's design by integrating the concept of "residual learning" and developing an effective method for training deep neural networks. Residual block attempts to tackle the issue of lowering gradient weight by training deep network. It became more accurate when ResNet-101 with 50 or more layers was used to categorize images.

3.2.3. Feature Selection Using Ant Colony System (ACS)

ACS is all about what ants do and how they move. As they move from one place to another, the ants spread a substance called "pheromone" that they leave behind. The strength of this material goes down over time. There is a good chance that the pheromone led the ants to the trail. This makes ants more likely to take the cheaper route. Accordingly, ants move from one place to another in the same way that points in a graph move from one point to another. A vertex is a feature, and an edge between two vertices is a choice about which feature to choose next. The method keeps trying different things to find the best ones. The approach stops when the least number of vertices have been reached and a freezing criterion has been met. The points are something that will happen at a certain point at a certain time. In general, the nth ant moves from state a to state b with the probability as shown in Equation (3).

$$p_{ab}^n = \frac{\left(Q_{ab}^\delta\right)\left(P_{ab}^\sigma\right)}{\sum allowed\left(\left(Q_{ab}^\delta\right)\left(P_{ab}^\sigma\right)\right)} \tag{3}$$

In Equaiton (3), $\left(Q_{ab}^\delta\right)$ is the amount of pheromone deposited for the switching state from a to b. δ is a parameter to control the change of $\left(Q_{ab}^\delta\right)$. σ is a parameter to control the change of $\left(P_{ab}^\sigma\right)$. $\left(Q_{ab}^\delta\right)$ and $\left(P_{ab}^\sigma\right)$ signify the trail level and desirability for the other possible state switches. Several of these features are insignificant for successful classification; hence, we used an efficient feature selection method known as the Ant Colony system to choose the most beneficial features to include in our classification. By the technique, these selected attributes are sent to SVM and its several SVM kernels for final classification.

4. Results and Discussion

In this segment, more detailed experiments are conducted to test the proposed framework. The following actions were performed to achieve the objectives: An image is enhanced using k-mean clustering, a deep CNN model that has been pre-trained is used for feature extraction, the best deep model features are selected using an Ant Colony system, and the best features are then concatenated for classification using SVM variants. In this study, the dataset known as fundus [43] is used. At the outset, each DR image was classified into one of three groups: non-referable DR (DR1, mild no proliferative DR), referable DR, and referable DR with proliferative features (RDR). A severity level of moderate no proliferative DR or worse, in addition to the presence of referable diabetic macular edema, was diagnostic of referable diabetic retinopathy (DME). The subtype of mild DR with no proliferative features is referred to as DR2, and it was differentiated from RDR. DR3 is the category that incorporates both proliferative and severe no proliferative DRs together in

one grouping as shown in Figure 3. The suggested method's performance is evaluated using several different metrics, including accuracy, total cost, prediction speed, training speed, precision, F1 rate, and recall rate among others. The experiments make use of five different folds.
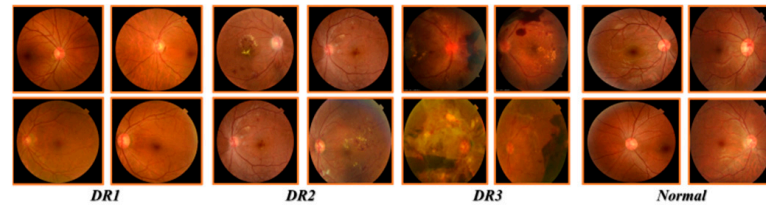

Figure 3. Fundus image database.

To determine whether the planned research would be successful, this study makes use of a variety of performance evaluation criteria. The confusion matrix that is generated during the testing procedure for the identification job is relied on by most of these methods. The calculations for these procedures are as follows: $Accuracy(Ac)$, $precision(Pe)$, $Recall(Re)$ & $F1\ Score(F1-s)$.

$$Ac = \frac{\text{TruePValues} + \text{TrueNValues}}{\text{TruePValues} + \text{TrueNValues} + \text{FalsePValues} + \text{FalseNValues}} \tag{4}$$

$$Re = \frac{\text{TruePValues}}{\text{TruePValues} + \text{FalseNValues}} \tag{5}$$

$$Pe = \frac{\text{TruePValues}}{\text{TruePValues} + \text{FalsePValues}} \tag{6}$$

$$F1-s = \frac{2*(Re*Pe)}{Re+Pe} \tag{7}$$

4.1. Experiment Setup 1 (250 Features)

In this experiment, 250 realistic attributes are used to evaluate a novel approach. The selected feature vector has a dimension of 250. Based on the feature set, DR and normal occurrences are classified using SVM classifiers. With a score of 92.6%, the C-SVM classifier performed the best in this evaluation. Q-SVM is the second-most accurate classifier. Table 1 provides an overview of the experiment's performance based on 250 criteria. The graph below depicts a true classifier, together with their corresponding training periods and prediction speeds (Figures 4 and 5). Figure 5 exhibited the confusion matrices relative to the classifier.

Table 1. Experiment Setup 1.

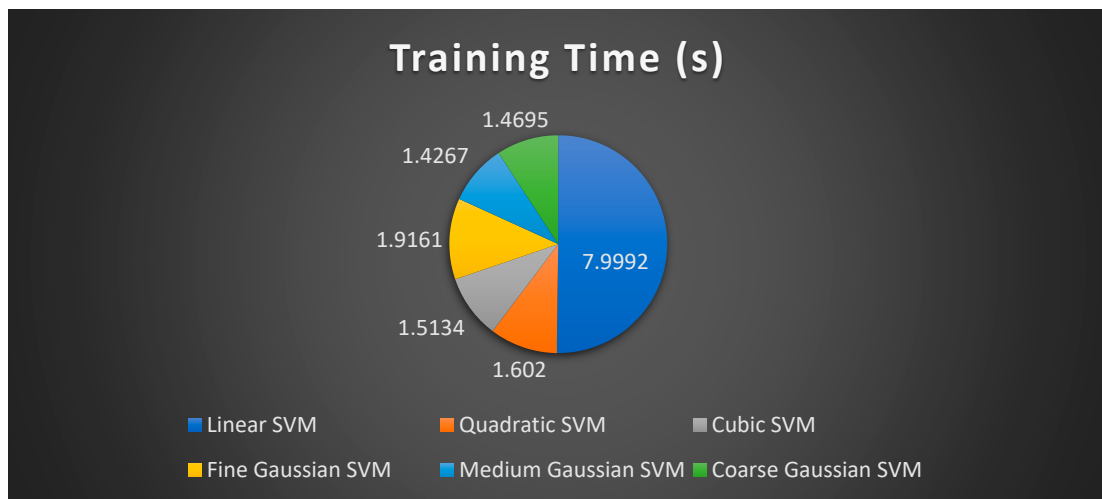| Classifier	Features	Accuracy (%)	Precision	Recall	F1 Score
Liner SVM	250	81.1	0.597	0.52	0.540
Quadratic SVM	250	92.3	0.957	0.955	0.955
Cubic SVM	250	92.6	0.922	0.937	0.927
Fine Gaussian SVM	250	41.3	0.33	0.592	0.282
Medium Gaussian SVM	250	87	0.852	0.882	0.862
Coarse Gaussian SVM	250	61.1	0.508	0.525	0.427

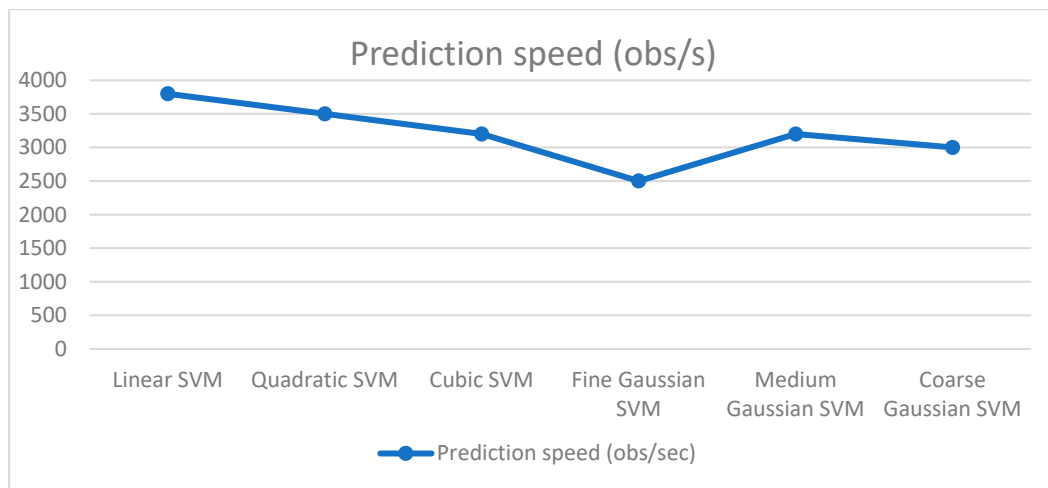**Figure 4.** Demonstrated training time of 250 features.

Figure 5. Demonstrated prediction speed of 250 features.

4.2. Experiment Setup 2 (550 Features)

This experiment tests a novel method on 550 features. The feature vector's dimension is 550. SVM classifiers distinguish DR from regular occurrences based on the feature set. The C-SVM classifier scored 91.8% overall. Q-SVM has the second-highest industry accuracy. Table 2 summarizes the experiment's 550-criteria performance. Figures 6 and 7 exhibit the training times and prediction speeds for a real classifier.

Table 2. Experiment Setup 2.

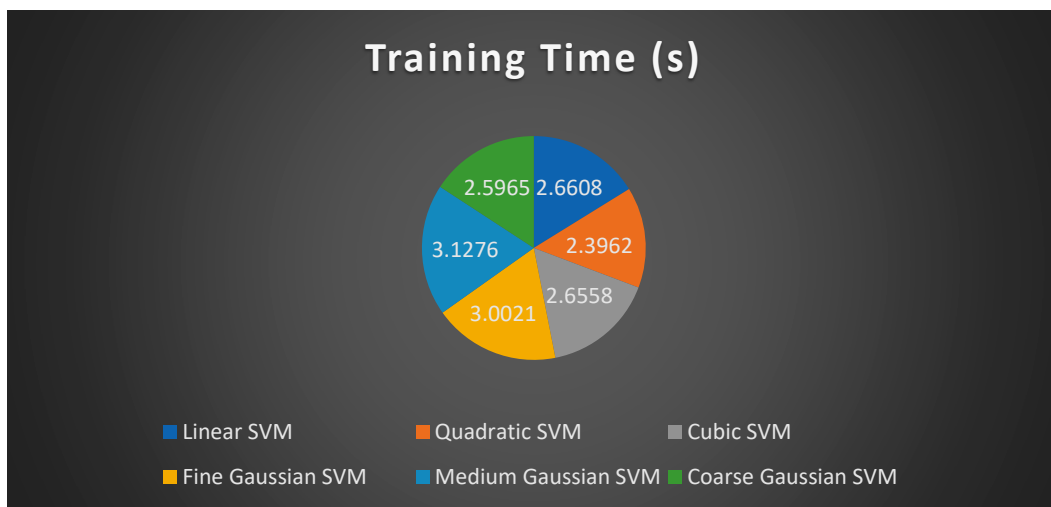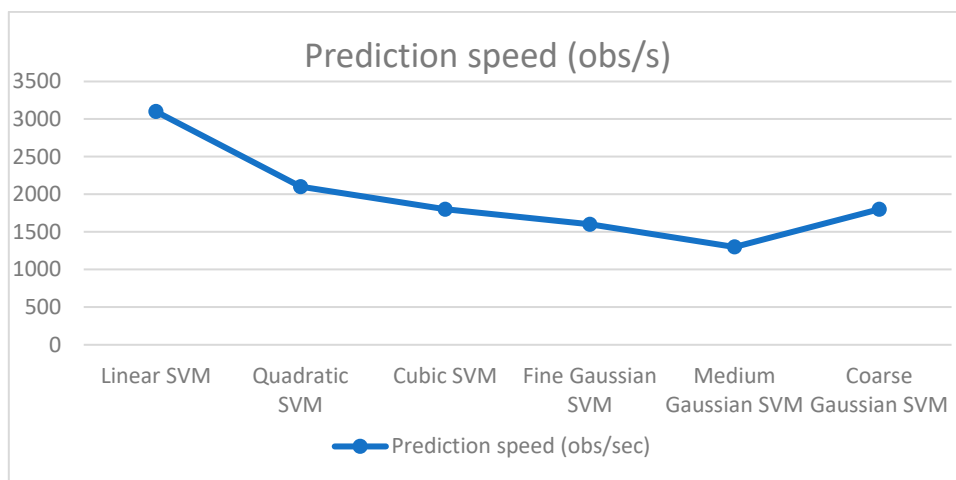| Classifier	Features	Accuracy (%)	Precision	Recall	F1 Score
Liner SVM	550	81.4	0.632	0.832	0.815
Quadratic SVM	550	91.1	0.91	0.92	0.912
Cubic SVM	550	91.8	0.915	0.93	0.917
Fine Gaussian SVM	550	41.7	0.345	0.842	0.422
Medium Gaussian SVM	550	88	0.655	0.83	0.647
Coarse Gaussian SVM	550	60.4	0.504	0.512	0.422

Figure 6. Training time of 550 features.

Figure 7. Prediction speed of 250 features.

4.3. Experiment Setup 3 (750 Features)

In this exercise, we experimented with a new approach on 750 random features. The 750-dimensional feature vector is picked. Feature set SVM classifiers identify DR outbreaks from regular occurrences. The C-SVM classifier won with 93% accuracy. Q-SVM has second-best accuracy. Table 3 summaries the trial's 750 outcomes. Figures 8 and 9 illustrate one classifier's training and prediction times.

Table 3. Experiment Setup 3.

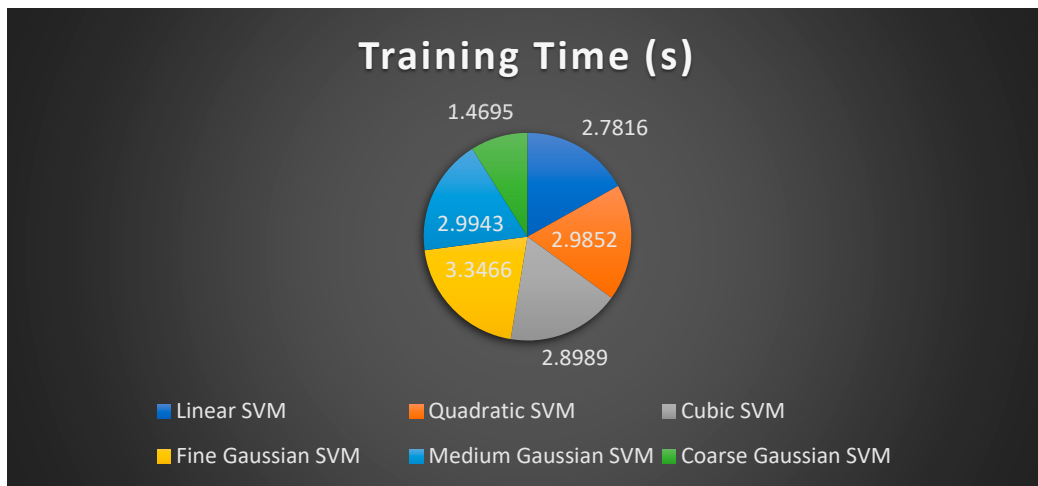| Classifier	Features	Accuracy (%)	Precision	Recall	F1 Score
Liner SVM	750	82.3	0.815	0.832	0.804
Quadratic SVM	750	92.6	0.93	0.932	0.93
Cubic SVM	750	93.0	0.93	0.935	0.932
Fine Gaussian SVM	750	40.8	0.64	0.842	0.286
Medium Gaussian SVM	750	87.9	0.857	0.897	0.872
Coarse Gaussian SVM	750	60.6	0.505	0.54	0.419

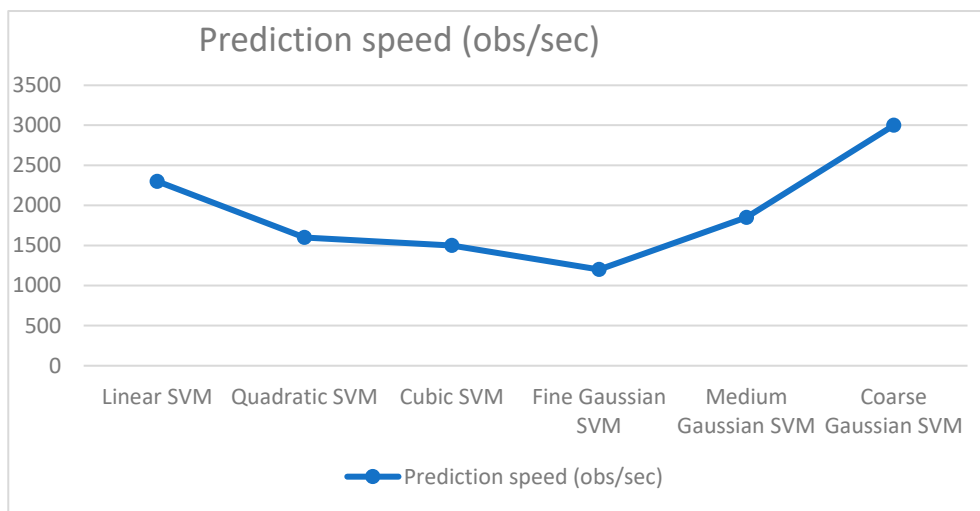**Figure 8.** Training time of 550 Features.

Figure 9. Prediction speed of 550 features.

4.4. Discussion

In this experiment, 250 real-world characteristics are utilized to assess a new method. The size of the chosen feature vector is 250. Using SVM classifiers, DR and normal occurrences are categorized based on the feature set. The C-SVM classifier fared the best in this examination, with a score of 92.6%. The second-most accurate classifier is Q-SVM. Based on 250 criteria, Table 1 presents a summary of the experiment's results. The graph below illustrates true classifiers along with their respective training times and prediction speeds. This experiment employs 550 characteristics to evaluate a unique technique. The dimension of the feature vector is 550. Using the feature set, the SVM classifiers identify DR from ordinary occurrences. Overall, the C-SVM classifier scored 91.8%. Q-SVM has the second-highest accuracy in the industry. The performance of the trial on 550 criteria is summarized in Table 2. We also tried a fresh method on 750 random characteristics in this experiment, selecting the 750-dimensional feature vector. Feature set SVM classifiers distinguish between DR outbreaks and common occurrences. The C-SVM classifier won with an accuracy of 93%. Q-SVM has the second-best precision. Table 3 summaries the 750 results of the experiment- listing normal, diabetic retinopathy, cataract, glaucoma, age-related macular degeneration, myopia, hypertension and other anomalies in fundus images from the Ocular Disease Intelligent Recognition (ODIR) collection. To enhance the dataset, left and right eye images were not differentiated, and these images were put on the VGG-16 CNN network to binary classify each condition independently. This research

compares the accuracy of each organ and the overall model to benchmark publications. Baseline accuracy rose from 89% to 91%, and the suggested approach enhanced illness identification.

Predictions of glaucoma, normal images, and other disorders have risen from 54% to 91% [44]. Table 4 shows a few comparisons with some of the previous techniques. Figure 10 shows the comparison of accuracy based on selected features (250, 550, and 750 etc.).

Table 4. Comparison from previous model.

|	Model	Results (%)	Dataset [43]
[45]	Transfer learning using VGG-16 No fusion (considered left and right images as separate images)	Validation Accuracy: 90.85 and F1-score: 91.0	Used all classes
Proposed	Fused features from fully connected layers of AlexNet and Resnet-101, after fusion used using ACS for core features selection for classification.	Accuracy = 93.0, Precision = 93.0, Recall = 93.5, F1-score = 93.2	Used Normal vs. DR1, DR2, and DR3
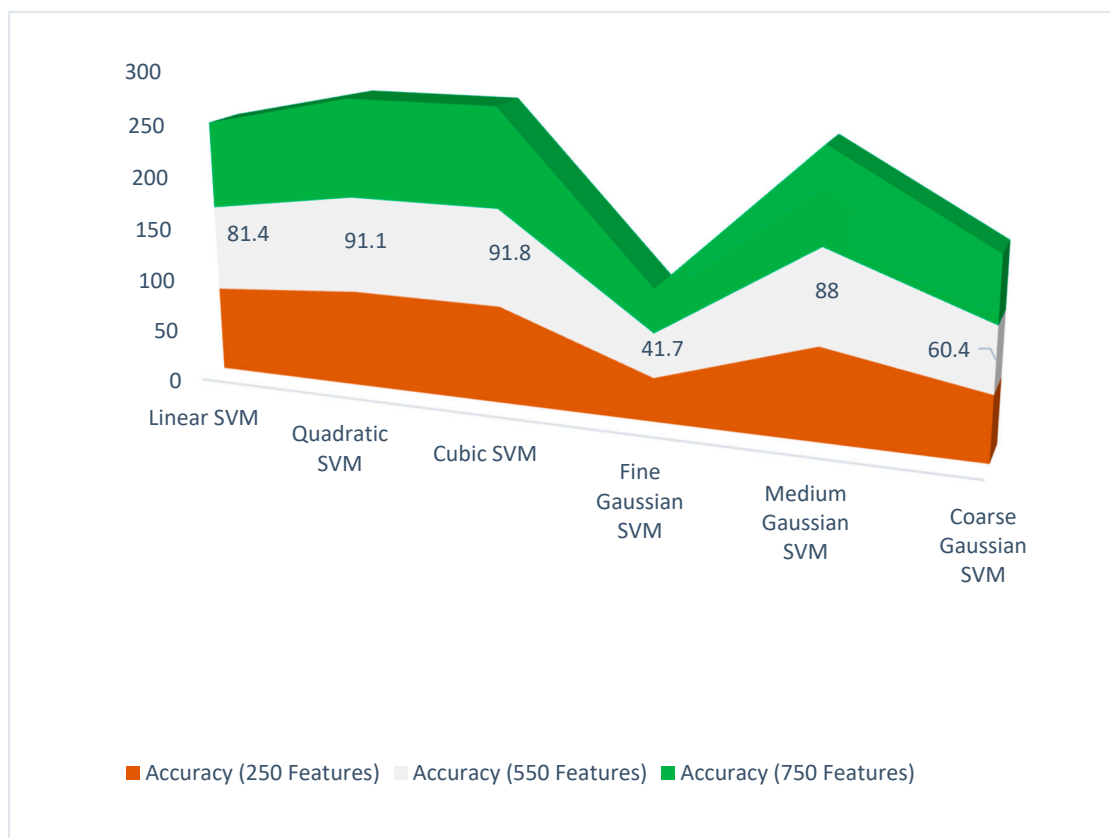
Figure 10. Assessment of accuracy based on features.

5. Conclusions

DR patients with delayed diagnosis and treatment are more likely to lose eyesight. Once early warning signals are recognized, the disease's severity must be confirmed before deciding on the best therapy. The proposition focuses on identifying DR fundus pictures by severity using a deep learning model. This paper presents a deep learning-based approach for categorizing fundus DR photos. Diabetic Retinopathy (DR), an eye condition caused by high blood glucose, has become more common. Diabetes affects over half the world's under-70 population. DR patients frequently lose eyesight without early diagnosis and treatment. After recognizing the warning indicators, the problem's severity must be confirmed to decide on treatment options. This work uses deep learning to classify DR fundus pictures

by severity. This paper presents a deep learning-based approach for classifying fundus DR pictures. In our proposition, feature extraction has been carried out promarily using AlexNet and Resnet101. Characteristics are collected from interdependent layers. Ant Colony systems help choose traits. Passing these qualities through an SVM with numerous kernels produces the final classification (SVM). Future efforts will focus on refining the DR classification by utilizing the latest deep learning algorithms instead of human grading to identify cases with diabetic retinopathy.

Author Contributions: Conceptualization, A.M.F. and M.I.S.; methodology, A.M.F. and S.A.; validation, S.A., A.K. and J.E.-D.; formal analysis, A.M.F. and M.I.S.; investigation, A.M.F.; resources, A.K. and M.I.S.; writing—original draft preparation, A.M.F., M.I.S. and A.K.; writing—review and editing, A.M.F., M.I.S. and A.K.; visualization, A.M.F., M.I.S. and A.K.; supervision, S.A.; project administration, S.A. and A.K. All authors have read and agreed to the published version of the manuscript.

Data Availability Statement: https://www.kaggle.com/c/diabetic-retinopathy-detection (accessed on 5 October 2022).

Conflicts of Interest: The authors declare no conflict of interest.

References

1. Kumar, A.; Tewari, A.S.; Singh, J.P. Classification of diabetic macular edema severity using deep learning technique. *Res. Biomed. Eng.* **2022**, *38*, 977–987. [CrossRef]
2. Heidari, A.; Jafari Navimipour, N.; Unal, M.; Toumaj, S. Machine learning applications for COVID-19 outbreak management. *Neural Comput. Appl.* **2022**, *34*, 15313–15348. [CrossRef] [PubMed]
3. Hayat, A.; Dias, M.; Bhuyan, B.P.; Tomar, R. Human Activity Recognition for Elderly People Using Machine and Deep Learning Approaches. *Information* **2022**, *13*, 275. [CrossRef]
4. Mateen, M.; Wen, J.; Song, S.; Huang, Z. Fundus image classification using VGG-19 architecture with PCA and SVD. *Symmetry* **2018**, *11*, 1. [CrossRef]
5. Alghamdi, H.S. Towards Explainable Deep Neural Networks for the Automatic Detection of Diabetic Retinopathy. *Appl. Sci.* **2022**, *12*, 9435. [CrossRef]
6. Shankar, K.; Zhang, Y.; Liu, Y.; Wu, L.; Chen, C.-H. Hyperparameter tuning deep learning for diabetic retinopathy fundus image classification. *IEEE Access* **2020**, *8*, 118164–118173. [CrossRef]
7. Farooq, U.; Sattar, N.Y. Improved automatic localization of optic disc in retinal fundus using image enhancement techniques and SVM. In Proceedings of the 2015 IEEE International Conference on Control System, Computing and Engineering (ICCSCE), Penang, Malaysia, 27–29 November 2015.
8. Boreiko, V.; Ilanchezian, I.; Ayhan, M.S.; Müller, S.; Koch, L.M.; Faber, H.; Berens, P.; Hein, M. Visual explanations for the detection of diabetic retinopathy from retinal fundus images. In *International Conference on Medical Image Computing and Computer-Assisted Intervention*; Springer: New York, NY, USA, 2022; pp. 539–549.
9. Bala, R.; Sharma, A.; Goel, N. Classification of Fundus Images for Diabetic Retinopathy Using Machine Learning: A Brief Review. In Proceedings of the Academia-Industry Consortium for Data Science, Wenzhou, China, 19–20 December 2020; Springer: Singapore, 2022; pp. 37–45.
10. Selvachandran, G.; Quek, S.G.; Paramesran, R.; Ding, W.; Son, L.H. Developments in the detection of diabetic retinopathy: A state-of-the-art review of computer-aided diagnosis and machine learning methods. *Artif. Intell. Rev.* **2022**, 1–50. [CrossRef]
11. Cao, J.; Felfeli, T.; Merritt, R.; Brent, M.H. Sociodemographics associated with risk of diabetic retinopathy detected by tele-ophthalmology: 5-year results of the Toronto tele-retinal screening program. *Can. J. Diabetes* **2022**, *46*, 26–31. [CrossRef]
12. Agarwal, S.; Bhat, A. A survey on recent developments in diabetic retinopathy detection through integration of deep learning. *Multimed. Tools Appl.* **2022**, 1–31. [CrossRef]
13. Li, T.; Bo, W.; Hu, C.; Kang, H.; Liu, H.; Wang, K.; Fu, H. Applications of deep learning in fundus images: A review. *Med. Image Anal.* **2021**, *69*, 101971. [CrossRef]
14. Xu, K.; Feng, D.; Mi, H. Deep convolutional neural network-based early automated detection of diabetic retinopathy using fundus image. *Molecules* **2017**, *22*, 2054. [CrossRef] [PubMed]
15. Sahlsten, J.; Jaskari, J.; Kivinen, J.; Turunen, L.; Jaanio, E.; Hietala, K.; Kaski, K. Deep learning fundus image analysis for diabetic retinopathy and macular edema grading. *Sci. Rep.* **2019**, *9*, 10750. [CrossRef] [PubMed]
16. Singh, L.K.; Garg, H.; Khanna, M. Deep learning system applicability for rapid glaucoma prediction from fundus images across various data sets. *Evol. Syst.* **2022**, *13*, 807–836. [CrossRef]
17. Go, S.; Kim, J.; Noh, K.J.; Park, S.J.; Lee, S. Combined Deep Learning of Fundus Images and Fluorescein Angiography for Retinal Artery/Vein Classification. *IEEE Access* **2022**, *10*, 70688–70698. [CrossRef]

18. Das, S.; Kharbanda, K.; Suchetha, M.; Raman, R.; Dhas, E. Deep learning architecture based on segmented fundus image features for classification of diabetic retinopathy. *Biomed. Signal Process. Control* **2021**, *68*, 102600. [CrossRef]

19. Kumar, N.S.; Radhika, Y. Optimized maximum principal curvatures based segmentation of blood vessels from retinal images. *Biomed. Res.* **2019**, *30*, 308–318. [CrossRef]

20. Bourne, R.R.; Stevens, G.A.; White, R.A.; Smith, J.L.; Flaxman, S.R.; Price, H.; Jonas, J.B.; Keeffe, J.; Leasher, J.; Naidoo, K. Causes of vision loss worldwide, 1990–2010: A systematic analysis. *Lancet Glob. Health* **2013**, *1*, e339–e349. [CrossRef]

21. Taylor, R.; Batey, D. *Handbook of Retinal Screening in Diabetes: Diagnosis and Management*; John Wiley & Sons: New York, NY, USA, 2012.

22. Lin, M.; Hou, B.; Liu, L.; Gordon, M.; Kass, M.; Wang, F.; Van Tassel, S.H.; Peng, Y. Automated diagnosing primary open-angle glaucoma from fundus image by simulating human's grading with deep learning. *Sci. Rep.* **2022**, *12*, 14080. [CrossRef]

23. Li, Z.; Guo, C.; Nie, D.; Lin, D.; Cui, T.; Zhu, Y.; Chen, C.; Zhao, L.; Zhang, X.; Dongye, M. Automated detection of retinal exudates and drusen in ultra-widefield fundus images based on deep learning. *Eye* **2022**, *36*, 1681–1686. [CrossRef]

24. Kundu, S.; Karale, V.; Ghorai, G.; Sarkar, G.; Ghosh, S.; Dhara, A.K. Nested U-Net for Segmentation of Red Lesions in Retinal Fundus Images and Sub-image Classification for Removal of False Positives. *J. Digit. Imaging* **2022**, *35*, 1111–1119. [CrossRef]

25. Bilal, A.; Zhu, L.; Deng, A.; Lu, H.; Wu, N. AI-Based Automatic Detection and Classification of Diabetic Retinopathy Using U-Net and Deep Learning. *Symmetry* **2022**, *14*, 1427. [CrossRef]

26. Canayaz, M. Classification of diabetic retinopathy with feature selection over deep features using nature-inspired wrapper methods. *Appl. Soft Comput.* **2022**, *128*, 109462. [CrossRef]

27. Islam, M.R.; Abdulrazak, L.F.; Nahiduzzaman, M.; Goni, M.O.F.; Anower, M.S.; Ahsan, M.; Haider, J.; Kowalski, M. Applying supervised contrastive learning for the detection of diabetic retinopathy and its severity levels from fundus images. *Comput. Biol. Med.* **2022**, *146*, 105602. [CrossRef] [PubMed]

28. Li, Z.; Xu, M.; Yang, X.; Han, Y. Multi-Label Fundus Image Classification Using Attention Mechanisms and Feature Fusion. *Micromachines* **2022**, *13*, 947. [CrossRef]

29. Atwany, M.Z.; Sahyoun, A.H.; Yaqub, M. Deep learning techniques for diabetic retinopathy classification: A survey. *IEEE Access* **2022**, *10*, 28642–28655. [CrossRef]

30. Agrawal, R.; Kulkarni, S.; Walambe, R.; Deshpande, M.; Kotecha, K. Deep dive in retinal fundus image segmentation using deep learning for retinopathy of prematurity. *Multimed. Tools Appl.* **2022**, *81*, 11441–11460. [CrossRef]

31. Li, F.; Wang, Y.; Xu, T.; Dong, L.; Yan, L.; Jiang, M.; Zhang, X.; Jiang, H.; Wu, Z.; Zou, H. Deep learning-based automated detection for diabetic retinopathy and diabetic macular oedema in retinal fundus photographs. *Eye* **2022**, *36*, 1433–1441. [CrossRef] [PubMed]

32. Saranya, P.; Prabakaran, S.; Kumar, R.; Das, E. Blood vessel segmentation in retinal fundus images for proliferative diabetic retinopathy screening using deep learning. *Vis. Comput.* **2022**, *38*, 977–992. [CrossRef]

33. Farooq, M.S.; Arooj, A.; Alroobaea, R.; Baqasah, A.M.; Jabarulla, M.Y.; Singh, D.; Sardar, R. Untangling computer-aided diagnostic system for screening diabetic retinopathy based on deep learning techniques. *Sensors* **2022**, *22*, 1803. [CrossRef]

34. Lalithadevi, B.; Krishnaveni, S. Detection of diabetic retinopathy and related retinal disorders using fundus images based on deep learning and image processing techniques: A comprehensive review. *Concurr. Comput. Pract. Exp.* **2022**, *34*, e7032. [CrossRef]

35. Butt, M.; Iskandar, D.; Abdelhamid, S.; Latif, G.; Alghazo, R. Diabetic Retinopathy Detection from Fundus Images of the Eye Using Hybrid Deep Learning Features. *Diagnostics* **2022**, *12*, 1607. [CrossRef] [PubMed]

36. Wang, Y.-S.; Tai, C.-L.; Sorkine, O.; Lee, T.-Y. Optimized scale-and-stretch for image resizing. In *ACM SIGGRAPH Asia 2008 Papers*; Association for Computing Machinery: New York, NY, USA, 2008; pp. 1–8.

37. Vassilvitskii, S.; Arthur, D. k-means++: The advantages of careful seeding. In Proceedings of the Eighteenth Annual ACM-SIAM Symposium on Discrete Algorithms, New Orleans, LA, USA, 7–9 January 2007; pp. 1027–1035.

38. Safdar, M.F.; Alkobaisi, S.S.; Zahra, F.T. A comparative analysis of data augmentation approaches for magnetic resonance imaging (MRI) scan images of brain tumor. *Acta Inform. Med.* **2020**, *28*, 29. [CrossRef]

39. Kamp, A. Vertical Flip. *Tex. Wesley. L. Rev.* **2006**, *13*, 729.

40. Russakovsky, O.; Deng, J.; Su, H.; Krause, J.; Satheesh, S.; Ma, S.; Huang, Z.; Karpathy, A.; Khosla, A.; Bernstein, M. Imagenet large scale visual recognition challenge. *Int. J. Comput. Vis.* **2015**, *115*, 211–252. [CrossRef]

41. Simonyan, K.; Zisserman, A. Very deep convolutional networks for large-scale image recognition. *arXiv* **2014**, arXiv:1409.1556.

42. He, K.; Zhang, X.; Ren, S.; Sun, J. Deep residual learning for image recognition. In Proceedings of the IEEE Conference on Computer Vision and Pattern Recognition, Las Vegas, NV, USA, 27–30 June 2016; IEEE: Las Vegas, NV, USA, 2016; pp. 770–778.

43. Cen, L.-P.; Ji, J.; Lin, J.-W.; Ju, S.-T.; Lin, H.-J.; Li, T.-P.; Wang, Y.; Yang, J.-F.; Liu, Y.-F.; Tan, S. Automatic detection of 39 fundus diseases and conditions in retinal photographs using deep neural networks. *Nat. Commun.* **2021**, *12*, 4828. [CrossRef]

44. Shamrat, F.M.J.M.; Azam, S.; Karim, A.; Islam, R.; Tasnim, Z.; Ghosh, P.; De Boer, F. LungNet22: A Fine-Tuned Model for Multiclass Classification and Prediction of Lung Disease Using X-ray Images. *J. Pers. Med.* **2022**, *12*, 680. [CrossRef]

45. Bali, A.; Mansotra, V. Transfer Learning-based One versus Rest Classifier for Multiclass Multi-Label Ophthalmological Disease Prediction. *Int. J. Adv. Comput. Sci. Appl.* **2021**, *12*, 537–546. [CrossRef]